MATERIALS CHEMISTRY FRONTIERS

CCS 中国化学会 CHINESE CHEMICAL SOCIETY

ICCAS

ROYAL SOCIETY OF CHEMISTRY

A pillararene-based supramolecular polymer hydrogel for removal of organic dyes from water

Journal:	*Materials Chemistry Frontiers*
Manuscript ID	QM-RES-09-2024-000793.R1
Article Type:	Research Article
Date Submitted by the Author:	21-Oct-2024
Complete List of Authors:	Ma, Jiaxin; Shanxi University Gong, Shanhao; Taiyuan University of Technology Cheng, Yujie; Shanxi University, Scientific Instrument Center Cao, Wei; Scientific Instrument Center, Shanxi University Wei, Xuehong; Shanxi University, Wang, Pi; Taiyuan University of Technology Xia, Danyu; Shanxi University

ARTICLE

A pillararene-based supramolecular polymer hydrogel for removal of organic dyes from water

Received 00th January 20xx,
Accepted 00th January 20xx

DOI: 10.1039/x0xx00000x

Jiaxin Ma,[a] Shanhao Gong,[b] Yujie Cheng,[a] Wei Cao,[a] Xuehong Wei,[a] Pi Wang,*[b] and Danyu Xia *[a]

Organic dyes in industrial wastewater are posing significant threats to global water resources and have raised concerns about negative impacts on human health. Hydrogels have attracted much attention among various absorbent materials due to their facile synthesis, high stability in water and large adsorption capacity. Herein, we have prepared a supramolecular polymer hydrogel adsorbent based on a water-soluble pillar[5]arene and poly(sodium 4-styrenesulfonate). Benefiting from pillararene, the hydrogel adsorbent can removal a variety of organic dyes from water. In particular, this hydrogel exhibited excellent adsorption properties for Eriochrome black T (EBT) with a much higher adsorption rate than activated carbon. Importantly, the adsorption capacity is as high as 1818 mg g^{-1}. Furthermore, the hydrogel adsorbent showed excellent selectivity and recyclability when adsorbing organic dyes from water. These excellent results showed the great potential of the pillararene-based supramolecular hydrogel adsorbent in water treatment.

Introduction

Organic dyes, widely utilized in various industries such as textile, leather, and cosmetics, serve as coloring and printing agents. However, the untreated organic dyes in wastewater are significant damages to environment and life.[1] Consequently, it is an imperative topic to separation and removal of organic dyes from wastewater in order to safeguard the environment and living organisms. Among the methods utilized for treatment of wastewater containing dyes, including photodegradation,[2] flocculation,[3] and ion exchange,[4] adsorption is notable for its efficiency, simplicity and economic viability.[5,6] Over the years, a variety of materials have been explored as adsorbents, including macrocycle-containing materials,[7,8] hydrogels,[9] layered double hydroxides,[10] metal-organic frameworks[11] and so on. Among these materials, hydrogels have attracted much attention because of their easy synthesis, high stability under high dyes loading and the ability to adsorb large quantities of water without dissolving.[12] Hydrogels possess covalent or noncovalent three-dimensional polymer networks, enabling them to retain large amounts of water through capillary action and surface tension.[13] This unique structure effectively increases the concentration of the adsorption sites, thereby enhancing the adsorption capacity, and making them excellent adsorbents for removal of dyes from water.[14]

Pillar[*n*]arenes,[15-20] a significant category of macrocycles, with electron-rich cavities, rigid structures and excellent host–guest properties, are ideal building blocks for constructing hydrogel adsorbents. Pillararene-based hydrogels can be obtained through chemical crosslinking and exploiting multiple supramolecular driving forces, such as π-π interaction, hydrogen bonding and host–guest interactions, stemming from the ease of functionalization of skeleton of pillararenes.[21-23]. The obtained hydrogels based on pillararenes combine the advantages of pillararenes and hydrogels, such as good mechanical properties, self-healing and multi-stimuli-responsiveness, which are excellent candidates for adsorption. For instances, Huang and coworkers prepared a hydrogel based on two pillar[5]arenes through Schiff base condensation, exhibiting excellent adsorption ability to multiple types of pollutants due to host–guest interactions facilitated adsorption between the pillar[5]arene macrocycles and pollutant molecules.[22] Hoogenboom and coworkers reported hydrogels with excellent tunable mechanical properties and water purification by covalently cross-linking linear polymers with a bifunctional macrocyclic pillar[5]arene, showing high adsorption performance for phenols and dyes such as methylene blue and methyl red.[24] Thongnuek and coworkers reported pillararene cross-linked gelatin hydrogels that can be used to control the uptake and release of antibiotics using light.[25]

Herein, we have prepared a supramolecular polymer hydrogel adsorbent based on pillararene with excellent capability towards removing organic dyes from water. The supramolecular polymer hydrogel was prepared from a water-soluble pilllar[5]arene (**WP5**) and poly (sodium 4-styrenesulfonate) (**PSS**) driven by electrostatic interaction (Scheme 1). The molar ratio of $(-N(CH_3)_3^+)/SO_3^-$ is 1:1, 1:2 and 1:10, corresponding to 10%, 5.0%, and 1.0 mol% **WP5**, to generate supramolecular polymer materials **SPH-1, SPH-2** and **SPH-3**, respectively. At the macroscope level, **SPH-1** and **SPH-2** formed hydrogels while **SPH-3** was a solution. In control, the

[a] Scientific Instrument Center, Shanxi University, Taiyuan 030006, P. R. China; orcid.org/0000-0001-6575-6448; Email: danyuxia@sxu.edu.cn
[b] College of Materials Science and Engineering, Taiyuan University of Technology, Taiyuan 030024, P. R. China; orcid.org/0000-0002-8803-7953; Email: wangpi@tyut.edu.cn

corresponding monomer **M** without pillar[5]arene skeleton cannot form hydrogels with **PSS**, indicating that pillararene cavity matters when forming hydrogels **SPH-1** and **SPH-2**. Compared to hydrogel **SPH-2**, **SPH-1** can remove organic dyes, orange G (OG), Eriochrome black T (EBT) and acid fuchsin (AF) from water with high efficiency. In addition, **SPH-1** can remove EBT with a much higher adsorption rate and capacity than those of activated carbon (AC). The adsorption capacity of EBT is as high as 1818 mg g^{-1}. Moreover, **SPH-1** showed excellent selectivity and recyclability when adsorbing organic dyes from water (Scheme 1).

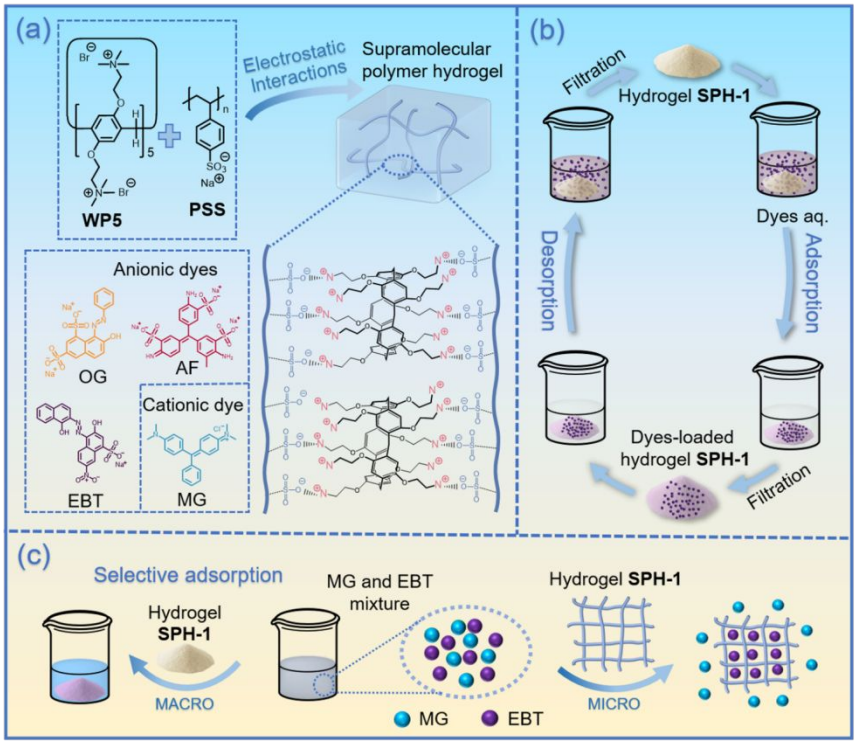

Scheme 1. (a) chemical structures of **WP5**, **PSS** and the related dyes and schematic illustration of the supramolecular polymer hydrogel; (b) Schematic illustration of the adsorption-desorption process of dyes by **SPH-1** and the regeneration of **SPH-1**; (c) Schematic illustration of the selectivity of **SPH-1**.

Experimental

Materials

All reagents and solvents were commercially available and used as supplied without further purification. The initial pH of dye solutions was adjusted with 0.1 M HCl or 0.1 M NaOH. All the analytical experiments were performed at room temperature (25.0 °C). ^{1}H NMR spectra were recorded on a Bruker Avance DMX 600 spectrophotometer. Scanning Electron Microscopy (SEM) investigations were obtained from a JEOL 6390LV instrument. UV–vis spectra were followed by a Hitachi UH5300 spectrophotometer. Thermogravimetric analysis (TGA) was accomplished on a METTLER TGA/DSC 1/1600 high temperature Thermogravimetric Analyser. Rheological testing was performed on MCR102 Advanced Rheology Expanded Systems. X-ray diffraction (XRD) measurements were carried out on a Bruker D2 PHASER instrument. The surface area was determined by Braunuer-Emmet-Teller (BET) method using a Micromeritics TriStar Ⅱ Plus 3030 instrument. Liquid nitrogen was used to measure the isotherms of N_2 adsorption and desorption at 77K.

SEM sample preparation

PSS, and **WP5** powders were vacuum dried and adhered to conductive tape to obtain SEM samples a and b. **SPH-1** and **SPH-2** powders were prepared by freeze-drying and adhered to conductive tape to obtain SEM samples c and d. **SPH-3** powders were vacuum dried and adhered to conductive tape to obtain SEM sample e.

Preliminary Dye removal experiments

The adsorption of dyes from water by **SPH-1** and **SPH-2** was studied using orange G (OG), Eriochrome black T (EBT), acid fuchsin (AF) and malachite green chloride (MG). All experiments were performed in deionized water at room temperature (25.0 °C) to evaluate the effect of adsorption parameters: dosage of absorbents (0.125–1.00 $g{\cdot}L^{-1}$) and Initial dyes concentration (5.00–100 $mg{\cdot}L^{-1}$). Initially, the absorbent powder was transferred to a 20.0 mL sample vial. The original dye solution (19.0 mL) was then added to the vial. The solution was stirred immediately, and 1.00 mL solution was drawn through syringe at the as-designed time. Subsequently, the suspension was filtered using an inorganic membrane filter made of PES with a pore size of 0.22 μm and a diameter of 13 mm. Finally, the residual concentration of the dye in each sample was determined using UV-vis spectroscopy. All dyes, except EBT, were diluted tenfold for UV-vis spectroscopy to prevent the instrument from hitting its upper detection limit.

Water content

The freeze-dried **SPH-1** was weighed to obtain the mass in the dried hydrogel state. Subsequently, the sample was immersed in deionized water for three hours, collected and drained of surface water with filter paper, and the hydrogel was weighed in its wet state. The water absorption was calculated using the following equation (1): [26]

$$\text{Water content} = \frac{W_s - W_d}{W_d} \times (1.)$$

where W_s (mg) and W_d (mg) represent the masses of the swollen hydrogel and the dried hydrogel, respectively.

Adsorption efficiency

The efficiency of dye removal (R%) by the adsorbent was determined using the following equation (2):[27]
where C_0 (mg·L^{-1}) is the original concentration of dye solution and C_t (mg·L^{-1}) is the residual concentrations of dye solution at time t (min).
Meanwhile, the amounts of adsorbed dye at time t (min) was calculated using the following equation (3):[28]

$$q_t = \frac{C_0 - C_t}{C_A} \times (2.)$$

where q_t (mg g^{-1}) is the amount of dye adsorbed by adsorbent at time t (min), C_0 (mg·L^{-1}) and C_t (mg·L^{-1}) are the original and residual concentration of dye solution at time t (min), respectively, and C_A (g L^{-1}) is the concentration of the adsorbent.

Adsorption kinetic study

Adsorption is a physicochemical process and can be quantified by several kinetic models. In this study, the pseudo-first-order model, pseudo-second-order model and the Weber and Morris intra-particle diffusion model were employed. These adsorption kinetics are expressed by the following equations (4), (5) and (6):[29]

$$ln(q_e - q_t) = lnq_e - k_1 t (3.)$$

$$\frac{t}{q_t} = \frac{t}{q_e} + \frac{1}{k_2 q_e^2} (4.)$$

$$q_t = k_i t^{0.5} + C (5.)$$

where q_t (mg g^{-1}) is the amount of dye adsorbed by adsorbent at time t (min) and q_e (mg g^{-1}) is the amounts of dye adsorbed by adsorbent at equilibrium, respectively, k_1 (min^{-1}), k_2 (g mg^{-1} min^{-1}) and k_i (mg g^{-1} min$^{0.5}$) stand for the pseudo-first-order model, pseudo-second-order model and the Weber and Morris intra-particle diffusion model rate constants, respectively. C represents a constant related to the thickness of boundary layer. All the constants above can be calculated by the linear fitting of the experimental data using the corresponding model.

Adsorption isotherm study

The adsorption isotherms were described by the Langmuir adsorption isotherm and the Freundlich adsorption isotherm models. The corresponding isotherm parameters can be calculated using the equations (7) and (8) as follows:[30]

$$\frac{C_e}{q_e} = \frac{1}{q_m K_L} + \frac{C_e}{q_m} (6.)$$

$$lnq_e = lnK_F + \frac{1}{n} lnC_e (7.)$$

Where K_L and K_F stand for the Langmuir constant and the Freundlich constant, respectively. n is a constant related to sorption intensity, and q_m is the maximum adsorption amount. C_e (mg·L^{-1}) is the residual dye concentrations of dye adsorbed by **SPH-1** at equilibrium and q_e (mg g^{-1}) is the amounts of dye adsorbed by **SPH-1** at equilibrium. All the constants above can be calculated by the linear fitting of the experimental data using the corresponding model.

Selective dye adsorption study

SPH-1 (1.00 g·L^{-1}) was added to the mixed solution of EBT (100 mg·L^{-1}) and MG (100 mg·L^{-1}) with a volume ratio of 1:1 to validate the selective adsorption performance. The concentration of the dye in the mixture before and after adsorption was determined using UV-vis spectroscopy.

Results and discussion

First, the formation of the supramolecular polymer hydrogel by different molar ratios of **WP5** and **PSS** was studied. The molar ratio of (-N(CH$_3$)$_3^+$)/SO$_3^-$ is 1:1, 1:2 and 1:10, corresponding to 10%, 5.0%, and 1.0 mol% **WP5**, to generate supramolecular polymer materials **SPH-1, SPH-2** and **SPH-3,** respectively (Table 1). As shown in Fig. S2 (ESI†), **SPH-1** and **SPH-2** formed hydrogel materials while **SPH-3** was a solution. In control, the corresponding monomer **M** without pillararene skeleton was used to prepare hydrogels (Fig. S1, ESI†). Without the pillararene skeleton, the control compound **M** cannot form hydrogels with **PSS** (Fig. S2, ESI†), indicating that pillararene cavity matters when forming hydrogels **SPH-1** and **SPH-2**.

Table 1 The formation of the related supramolecular materials

Components	Molar ratios	Molar ratios of N(CH$_3$)$_3^+$/SO$_3^-$	Abbreviations	Statuses
WP5 and **PSS**	1:10	1:1	**SPH-1**	hydrogel
WP5 and **PSS**	1:20	1:2	**SPH-2**	hydrogel
WP5 and **PSS**	1:100	1:10	**SPH-3**	solution
M and **PSS**	1:2	1:1	**M1**	solution
M and **PSS**	1:4	1:2	**M2**	solution
M and **PSS**	1:20	1:10	**M3**	solution

Since **SPH-1** and **SPH-2** are insoluble in water, we utilized the water-soluble **SPH-3** as a model material to study the formation of the hydrogels by ^{1}H NMR spectroscopy. As shown in Fig. S3 (ESI†), the peaks related to the protons H_1 and H_2 shifted upfield and became broad and some of signal for the proton H_a on **PSS** shifted downfield, indicating the formation of hydrogel driven by electrostatic interaction between **WP5** and **PSS**. The morphology of the hydrogels was investigated by scanning electron microscopy (SEM). As shown in Fig. 1a, **PSS** powder exhibited spherical structures. The hydrogel **SPH-1** showed three-dimensional network structure with rough surface (Fig. 1d). **WP5**, **SPH-2** and **SPH-3** powders showed layered structures (Fig. 1b, 1e and 1f). The morphology changed as the **WP5**

content increased, suggesting the effect of **WP5** on the morphology of the obtained hydrogels.

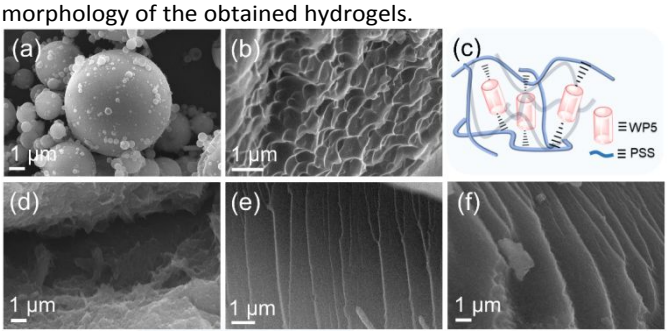

Fig. 1 SEM images: (a) **PSS**; (b) **WP5**; (d) **SPH-1**; (e) **SPH-2**; (f) **SPH-3**; (c) illustration of the supramolecular polymer hydrogels.

Rheological studies were conducted to analyze the mechanical properties of the hydrogels **SPH-1** and **SPH-2**. The fully swollen supramolecular polymer hydrogels exhibit high mechanical strength ranging from 10 kPa to 1000 kPa. The dynamic strain sweep curves demonstrated that *G*′ consistently exceeded *G*′′ at strains ranging from 0.001% to 1% (Fig. 2a). The dynamic frequency sweep curves indicated that *G*′ was larger than *G*′′ at the fixed 1% strain (Fig. 2b), indicating the formation of the hydrogels **SPH-1** and **SPH-2**. As expected, the mechanical strength of **SPH-1** was greater than that of **SPH-2**, which was attributed to the higher cross-linking density of the hydrogel with larger content of **WP5**.[24] Using the freeze-drying method, the solvent content of **SPH-1** was calculated to be 72.7% (Table S1), indicating its favorable hydrophilicity. Additionally, the TGA data showed that **SPH-1** began to decompose at 280 °C. suggesting excellent thermal stability (Fig. S4, ESI†). As shown in Fig. S5, the specific surface area of the adsorbent **SPH-1** determined by the Brunauer–Emmett–Teller (BET) method was 4.895 m^2/g, indicating nonporous structure (Fig. S5, ESI†). Moreover, the powder X-Ray diffraction pattern of the hydrogel exhibited a broad peak at 2θ = 20° (Fig. S6, ESI†), suggesting that **SPH-1** possessed an amorphous structure and non-crystalline state.

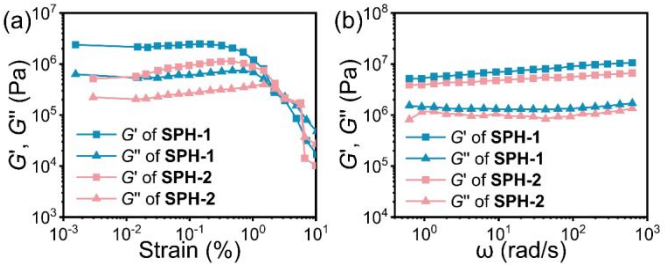

Fig. 2 Variation of storage modulus (*G*′) and loss modulus (*G*′′) of **SPH-1** and **SPH-2** hydrogel as a function of (a) strain and (b) angular frequency at 25.0 °C.

To evaluate the adsorption behavior of **SPH-1** and **SPH-2** to dyes, several typical pollutants found in textile industry wastewater, orange G (OG), Eriochrome black T (EBT), acid fuchsin (AF) and malachite green chloride (MG) were chosen. Among them, OG, EBT, AF are anionic dyes and MG is a cationic dye. The residual concentrations of the dye were measured at different time intervals using UV-vis spectroscopy. **SPH-1** showed high adsorption efficiency towards OG, AF and EBT (Fig. S7, ESI†). Among them, **SPH-1** demonstrated the highest efficiency in EBT removal, of which 99.66% was removed within 2 min (Fig. 3a and 3b). Meanwhile, at the same conditions, **SPH-1** has a higher dye adsorption capacity than **SPH-2**. The adsorption of EBT by **SPH-2** reached equilibrium at 300 minutes with an adsorption efficiency of only 60.63% (Fig. 3c and S8 ESI†), indicating the importance of pillararene in the hydrogel adsorbents. In addition, **SPH-1** exhibited excellent adsorption properties to the anionic dyes while almost no adsorption effect towards MG (Fig. S7a, ESI), owing to the electrostatic repulsion between the positively charged hydrogel and cationic MG.

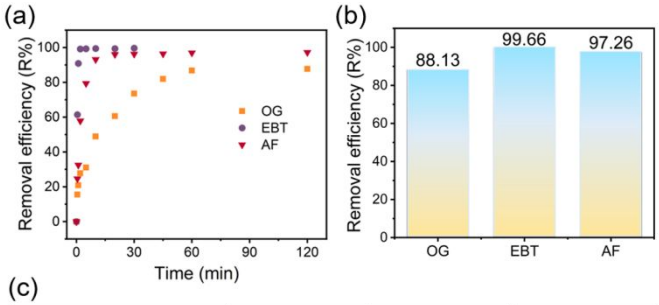

(c)

	OG		EBT		AF		MG	
	R_e (%)	t_e (min)	R_e (%)	t_e (min)	R_e (%)	t_e (min)	R_e (%)	t_e (min)
SPH-1	87.96	120	99.66	2	97.26	60	--------	--------
SPH-2	--------	--------	60.63	300	34.87	1440	--------	--------

Fig. 3 (a) The time-dependent adsorption efficiency of OG, AF, EBT by **SPH-1**. (b) The removal efficiency of OG, AF, EBT by **SPH-1** at equilibrium. (c) Adsorption efficiency (R_e) and equilibrium time (t_e) of **SPH-1**, **SPH-2** towards organic dyes. "--------" means no adsorption effect.

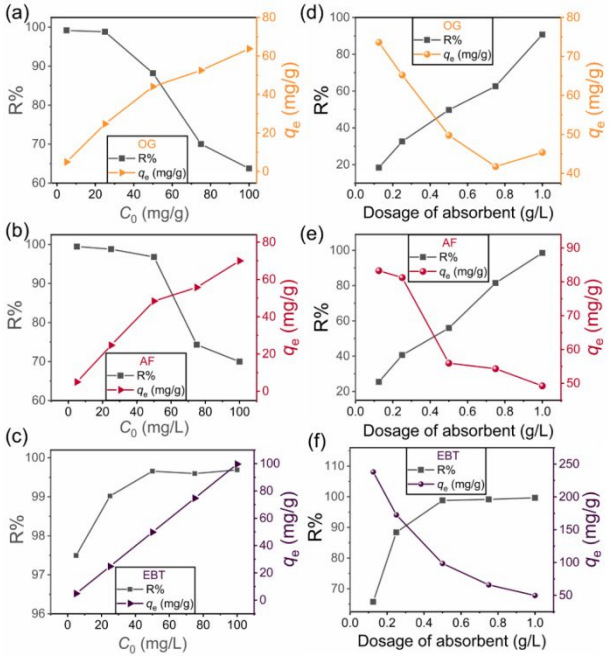

Fig. 4 Effect of initial dye concentrations on the adsorption efficiency and adsorption capacity of **SPH-1** with (a) OG, (b) AF and (c) EBT, T = 25.0 °C, pH = 7.0, C_A = 1.00 g/L, *t* = 36 h; Effect of **SPH-1** dose on adsorption efficiency and adsorption with (e) OG, (f) AF and (g) EBT, T = 25.0 °C, pH = 7.0, C_0 = 50.0 mg/L, *t* = 36 h.

The effects of adsorbent dosage and initial dye concentrations on the adsorption of the dyes by **SPH-1** were investigated. As the initial concentration of the dyes increased from 5.00 to 100 mg/L, the adsorption capacity of **SPH-1** to the dyes OG and AF increased while the adsorption efficiency decreased (Fig. 4a and 4b). This phenomenon was attributed to the excess of dye molecules at the high initial concentration, enhancing mass transfer with the active sites on the surface of the adsorbent. However, the limited number of active sites on the surface of the adsorbent could not bind with the remaining dye molecules, leading to a decrease in adsorption efficiency.[31] On the other hand, the adsorption capacity and efficiency of **SPH-1** were observed to increase with the initial concentration of EBT (Fig. 4c), suggesting that the dye concentration has not yet approached the maximum adsorption capacity of **SPH-1** for EBT. This result indicates that **SPH-1** exhibits excellent adsorption performance on EBT. The dosage of adsorbent is also an important parameter in the adsorption process of dyes. With the increase of adsorbent dosage up to 1.00 g/L, the removal rate of each dye by **SPH-1** increased to nearly 100%, but the adsorption capacity kept decreasing (Fig. 4d-f). This phenomenon can be explained by the availability of empty active sites of the adsorbent.[32] The available adsorption sites increased with the increasing **SPH-1** dosage. However, at a higher **SPH-1** dosage, even though more active sites were available for adsorption, the adsorption easily reached equilibrium due to the osmotic pressure, which resulted in poor active site utilization.[33] Taken together, an initial dye concentration of 50.0 mg/L and an adsorbent dosage of 1.00 g/L were selected for subsequent experiments.

Table 2 Rate parameters and linear regression correlation coefficients of the pseudo-first-order model, the pseudo-second-order model and the Weber and Morris intraparticle diffusion model of **SPH-1** in adsorption

	The pseudo-first-order model		The pseudo-second-order-model		The Weber and Morris model								
Dyes	K_1 (min^{-1})	R^2	K_2 ($g \cdot mg^{-1} \cdot min^{-1}$)	R^2	k_i ($mg \cdot g^{-1} \cdot min^{0.5}$)	C	R^2	k_i ($mg \cdot g^{-1} \cdot min^{0.5}$)	C	R^2	k_i ($mg \cdot g^{-1} \cdot min^{0.5}$)	C	R^2
OG	0.04548	0.9721	0.001433	0.9821	5.549	-1.586	0.9922	3.966	9.942	0.9466	1.002	32.97	0.7288
EBT	0.5452	0.6406	0.1996	0.9998	22.90	-18.36	0.8257	0.01414	49.36	0.9597			
AF	0.1574	0.7075	0.01939	0.9986	18.17	-1.601	0.9950	0.4119	47.88	0.9401			

Adsorption is a physicochemical process, the adsorption of dyes can be assumed as the following three consecutive stages: 1) boundary layer diffusion: Dye molecules pass from the inside of the solution to the outer surface of the adsorbent by convective diffusion; 2) intra-particle diffusion: the dye molecules penetrate the micropores of the adsorbent from the outer surface of the adsorbent and then diffuse to the inner surface of the adsorbent; 3) the combination of adsorbates and active sites.[34] The pseudo-first-order model, pseudo-second-order model, and Weber-Morris intra-particle diffusion model were applied to explore the interactions between the liquid-phase and adsorbent interfaces in the adsorption process. As shown in Table 2, the coefficient (R^2) values for the pseudo-second-order model are closer to 1 compared with the pseudo-first-order model (Fig. S9 and S10, ESI†), suggesting that the adsorption process of dyes by **SPH-1** can be approximately explained by pseudo-second-order model. The adsorption process of these dyes involves interactions between specific active sites on the adsorbent and the dye molecules, which is the rate-controlling step in adsorption.[35] In general, the adsorption rate is controlled by boundary layer diffusion or intra-particle diffusion. The Weber and Morris model describes that intraparticle diffusion controls the adsorption process if the plot of q_t versus $t^{0.5}$ is a straight line. To identify the rate-controlling step of the adsorption process, we applied the Weber-Morris model to processing the adsorption data. As depicted in Fig. S11 (ESI†), the fitting plot of q_t versus $t^{0.5}$ showed multiple different straight lines, indicating the presence of at least two adsorption processes. The first line has a steep slope, indicating that the rate-limiting step in this phase is surface diffusion, which involves the movement of dye molecules from the external solution into the boundary layer of **SPH-1**.[36] The second line has a considerably smaller slope, suggesting that the rate-controlling step in this phase could be either intra-particle diffusion or pore diffusion (or both).[37] However, neither line passes through the origin, indicating that intra-particle diffusion is not the sole rate-controlling step.[22] Furthermore, the Langmuir and Freundlich isotherm models were utilized to elucidate the interaction between **SPH-1** and dyes. The obtained parameters from the Langmuir and Freundlich equations can be found in Table 3. The Langmuir isotherm model exhibited higher correlation coefficients than the Freundlich model (Fig. S12 and S13, ESI†). This suggests that the adsorption behaviour of **SPH-1** is consistent with the typical adsorption process in non-porous solids in which dyes are adsorbed onto the uniform monolayer surface of the adsorbent.[38] **SPH-1** possesses numerous uniform adsorption sites on its surface that exhibit equal adsorption affinities. Occupying one active site does not affect its neighbouring sites. Notably, **SPH-1** exhibited a maximum adsorption capacity towards EBT (1310 mg g^{-1}). Hence, we pursued a subsequent study utilizing EBT.

Table 3 The adsorption isotherm parameters obtained from isotherm models fitting to the experimental data of **SPH-1** in adsorption

Dyes	Langmuir isotherm model			Freundlich isotherm model		
	K_L (L mg^{-1})	q_m (mg g^{-1})	R^2	K_F (L mg^{-1})	n	R^2
OG	0.3696	84.03	0.9988	23.42	4.539	0.8317
EBT	0.05091	1310	0.9981	99.15	1.625	0.9715
AF	0.2788	108.7	0.9904	45.36	5.005	0.8664

Industrial wastewater containing dyes carry different electrolytes that notably elevate the ionic strength and impact

the efficiency of the adsorption process. The adsorption of EBT by **SPH-1** was evaluated by varying the ionic strength using NaCl (Fig. S14, ESI†). The value of the adsorption efficiency without NaCl is 99.66%. With the increase of the NaCl concentration to 6.00 g/L, the adsorption efficiency can be kept at 95.37%. When the concentration of NaCl continually increased to 10.0 g/L, the adsorption efficiency declined to 71.94%. There may be a competition effect between the excess anions present in the system (Cl^-) and the EBT molecules.[39] This phenomenon is also probably caused by dimerization and aggregation of azo dye molecules as increase in the concentration of electrolytes in dye solution (Fig. S15, ESI†).[40] The adsorption efficiency decreased significantly when the concentration of NaCl was 4.0 g/L, indicating that the adsorption phenomenon of **SPH-1** was disturbed only at high ionic strength.

The pH of the dye solution was a non-negligible factor that affected the process of adsorption. The adsorption behaviour of **SPH-1** for EBT as the pH values increased from 2 to 12 was studied. There is a slight decrease trend in the adsorption efficiency as pH value increased (Fig. S16, ESI†). The points of zero charge (PZC) of **SPH-1** had played an imperative role in the adsorption capacity of EBT at different pH concentration.[41, 42] The pH value of PZC (pH_{PZC}) of **SPH-1** is determined to be 5.16 (Fig. S17, ESI†). For **SPH-1**, the active sites are ($-N(CH_3)_3^+$) from pillararene, the adsorbent surface charge density increases due to the rise in H^+ at pH < pH_{PZC}, resulting in an enhanced electrostatic interaction with EBT molecules and an increase of the adsorption efficiency.[43] The highest adsorption efficiency was observed at pH = 3.0 (Fig. S16, ESI†). The electrostatic interaction between EBT and **SPH-1** was decreased as the formation of negative active sites on the adsorbent surface at pH > pH_{PZC}, leading to a decrease in EBT absorption efficiency. The results support that the electrostatic interaction between the dyes and **SPH-1** act as the main factor for the effective adsorptive removal from wastewater samples. Next, we studied the adsorption properties of **SPH-1** with EBT dye at pH = 3.0 (Fig. S18, S19 and S20, ESI†). Using the Langmuir adsorption equation, we obtained the maximum adsorption amounts of the adsorbent at equilibrium for EBT. **SPH-1** exhibited a maximum adsorption capacity towards EBT (1818 mg g^{-1}). To the best of our knowledge, this is probably the highest adsorption capacity ever reported for EBT, which was obtained by using pillararene-based hydrogel adsorbent (Table 4).

Table 4 Comparison of adsorption capacity of other adsorbent materials for EBT in recent years

Adsorbent materials	Adsorption capacity (mg g^{-1})
Chemically modified steel slags[33]	119.0
Zinc oxide nanoparticles[44]	78.34
Cationic dialdehyde cellulose microfibers[39]	563.3
Magnetic graphene oxide (MGO)[45]	210.5
DPA-MgAl-LDH[46]	425.2
Chitosan Magnetic bioadsorbents[47]	280.0
Biochar/Layered double Hydroxide/Chitosan hybrid composite[43]	806.4
This work	1818

The applicability of **SPH-1** for removing EBT from various water samples with a known concentration of the dye was investigated. Samples were collected from diverse sources, including the rain water, Fenhe river, and Jinyang lake.[48, 49] Each sample was spiked with 50.0 mg·L^{-1} of EBT, and adsorption experiments were conducted under optimized conditions. As shown in Fig. S12, **SPH-1** exhibited the adsorption efficiencies as 99.99%, 97.90%, 98.20%, 99.66% towards EBT from rain water, Fenhe river water, Jinyang lake water and deionized water, respectively (Fig. S12, ESI†). These results indicate the potential application of the supramolecular polymer hydrogel **SPH-1** in environmental remediation.

The selective separation performance of the hydrogel adsorbent was studied considering the great difference between the adsorption performance of **SPH-1** to anionic EBT and cationic MG. As shown in Fig. 5a, **SPH-1** was added to the mixed solution of EBT and MG. The colour of the mixed solution changed from blueviolet to aquamarine after 5 min. Meanwhile, the characteristic adsorption peak of EBT in the UV–vis spectra almost completely disappeared, which were run in quadruplicate (Fig. 5b and S22, ESI†). These results indicated that **SPH-1** can selectively adsorb anionic EBT from the mixture of EBT and MG. In addition, the removal efficiency of **SPH-1** for EBT is similar compared to AC, but **SPH-1** has a higher adsorption rate. **SPH-1** can almost completely remove EBT in 2 minutes with an adsorption efficiency of 99.66%, while AC requires 300 minutes to reach equilibrium with an adsorption efficiency of 97.61% (Fig. 5c, S23 and S24, ESI†). Using the Langmuir adsorption equation, we obtained the maximum adsorption amounts of AC towards EBT was only 478.5 mg·g^{-1} (Fig. S25, ESI†). Further, following the adsorption study of the EBT, the adsorbent was desorbed by stirring it in 100 mL of saturated NaOH ethanol solution for 3 hours. The desorbed adsorbent was then subjected to centrifugation at 4,000 rpm. The precipitate was then rinsed with deionized water, and finally vacuum dried at 40 °C overnight to obtain the hydrogel adsorbent. After each round of desorption, the adsorbent was weighed and used for the next adsorption-desorption experiment. As shown in Fig. 5d, the **SPH-1** has no obvious performance loss after 5 consecutive cycle tests of adsorbing EBT, proving its good recyclability. Therefore, compared with those reported adsorbents in Table 4 for the removal of EBT, **SPH-1** showed some advantages including facile preparation, high adsorption capacity, wide pH range of applicability and excellent recyclability.

Conclusions

In summary, a supramolecular polymer hydrogel **SPH-1** has been successfully prepared based on a water-soluble pillar[5]arene and poly(sodium 4-styrenesulfonate). The hydrogel **SPH-1** can act as an excellent adsorbent for removal of organic dyes from water, including orange G (OG), Eriochrome black T (EBT) and acid fuchsin (AF). Especially for EBT, the adsorption capacity is as high as 1818 mg g^{-1}. Specifically, **SPH-1** exhibits superior adsorption rate and adsorption capacity compared to commercial activated carbon. Moreover, the hydrogel showed excellent selectivity and can be regenerated

via a simple washing method with almost no loss in performance after five cycles. This work provides an effective and economical way to prepare hydrogel adsorbents by pillararene and might stimulate wide interest of scientists for further development of new pillararene-based supramolecular hydrogels.

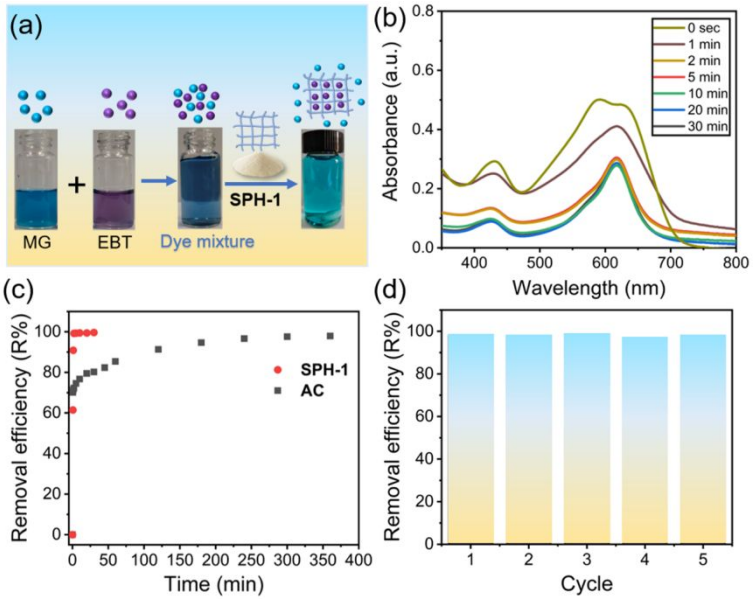

Fig. 5 (a) The selective adsoprtion experiment of **SPH-1**; (b) UV–vis spectra of the mixed solution EBT + MG (50.0 mg L^{-1} for each) before and after adsorption by **SPH-1**. (c) Time-dependent removal of EBT by **SPH-1** and AC. (d) Five regeneration cycles of **SPH-1** after the adsorption of EBT by washing at room temperature.

Conflicts of interest

There are no conflicts to declare.

Acknowledgements

This work was supported by the National Science Foundation for Young Scientists of China (21901149), the General Program of Natural Science Foundation of Shanxi Province, China (202103021224072 and 202303021211005) and the Natural Science Foundation for Young Scientists of Shanxi Province, China (202203021212480).

References

1 J. Lin, W. Ye, M. Xie, D. H. Seo, J. Luo, Y. Wan and B. Van der Bruggen, Environmental impacts and remediation of dye-containing wastewater, *Nat. Rev. Earth Environ.*, 2023, **4**, 785-803.

2 C. Alberoni, I. Barroso-Martín, A. Infantes-Molina, E. Rodríguez-Castellón, A. Talon, H. Zhao, S. You, A. Vomiero and E. Moretti, Ceria doping boosts methylene blue photodegradation in titania nanostructures, *Mater. Chem. Front.*, 2021, **5**, 4138-4152.

3 S. Ihaddaden, D. Aberkane, A. Boukerroui and D. Robert, Removal of methylene blue (basic dye) by coagulation-flocculation with biomaterials (bentonite and Opuntia ficus indica), *J. Water Process Eng.*, 2022, **49**, 102952.

4 M. A. Alkhadra, X. Su, M. E. Suss, H. Tian, E. N. Guyes, A. N. Shocron, K. M. Conforti, J. P. de Souza, N. Kim, M. Tedesco, K. Khoiruddin, I. G. Wenten, J. G. Santiago, T. A. Hatton and M. Z. Bazant, Electrochemical Methods for Water Purification, Ion Separations, and Energy Conversion, *Chem. Rev.*, 2022, **122**, 13547-13635.

5 P. Lu, J. Cheng, Y. Li, L. Li, Q. Wang and C. He, Novel porous β-cyclodextrin/pillar[5]arene copolymer for rapid removal of organic pollutants from water, *Carbohydr. Polym.*, 2019, **216**, 149-156.

6 Y. Liang, X. Yang, X. Wang, Z.-J. Guan, H. Xing and Y. Fang, A cage-on-MOF strategy to coordinatively functionalize mesoporous MOFs for manipulating selectivity in adsorption and catalysis, *Nat. Commun.*, 2023, **14**, 5223.

7 A. Alsbaiee, B. J. Smith, L. Xiao, Y. Ling, D. E. Helbling and W. R. Dichtel, Rapid removal of organic micropollutants from water by a porous β-cyclodextrin polymer, *Nature*, 2016, **529**, 190-U146.

8 P. Niu, C. Shi, J. Jiao, W. Xie, H. Qiu, Z. Yang, J. Jiang and L. Wang, Synthesis of Tröger's base-based [3]arenes for efficient iodine adsorption, *Chem. Commun.*, 2023, **59**, 10960-10963.

9 X.-T. Wang, X. Deng, T.-D. Zhang, X. Zhang, W.-P. Shi, J. Lai, H. Zhou, Y.-J. Ye, C.-Y. Zhang and D.-C. Yin, Biocompatible self-healing hydrogels based on boronic acid-functionalized polymer and laponite nanocomposite for water pollutant removal, *Environ. Chem. Lett.*, 2022, **20**, 81-90.

10 X. Wang, B. Cheng, L. Zhang, J. Yu and Y. Li, Synthesis of MgNiCo LDH hollow structure derived from ZIF-67 as superb adsorbent for Congo red, *J. Colloid Interface Sci.*, 2022, **612**, 598-607.

11 U. Patel, B. Parmar, P. Patel, A. Dadhania and E. Suresh, The synthesis and characterization of Zn(ii)/Cd(ii) based MOFs by a mixed ligand strategy: a Zn(ii) MOF as a dual functional material for reversible dye adsorption and as a heterogeneous catalyst for the Biginelli reaction, *Mater. Chem. Front.*, 2021, **5**, 304-314.

12 Z. Zhang, S. S. Rumi, L. A. Lucia and N. Abidi, Transforming low-quality cotton fibers into dye adsorbents, *Environ. Chem. Lett.*, 2024, **22**, 981-987.

13 Z. Wu, P. Zhang, H. Zhang, X. Li, Y. He, P. Qin and C. Yang, Tough porous nanocomposite hydrogel for water treatment, *J. Hazard. Mater.*, 2022, **421**, 126754.

14 Y. Hua, D. Xu, Z. Liu, J. Zhou, J. Han, Z. Lin, D. Xu, G. Chen, X. Huang, J. Chen, J. Lv and G. Liu, Effective adsorption and removal of malachite green and Pb2+ from aqueous samples and fruit juices by pollen–inspired magnetic hydroxyapatite nanoparticles/hydrogel beads, *J. Cleaner Prod.*, 2023, **411**, 137233.

15 Y. Wu, M. Tang, Z. Wang, L. Shi, Z. Xiong, Z. Chen, J. L. Sessler and F. Huang, Pillararene incorporated metal–organic frameworks for supramolecular recognition and selective separation, *Nat. Commun.*, 2023, **14**, 4927.

16 M. Li, Y. Liu, L. Shao, B. Hua, M. Wang, H. Liang, N. M. Khashab, J. L. Sessler and F. Huang, Pillararene-Based Variable Stoichiometry Co-Crystallization: A Versatile Approach to Diversified Solid-State Superstructures, *J. Am. Chem. Soc.*, 2023, **145**, 667-675.

17 M.-H. Li, Z. Yang, H. Hui, B. Yang, Y. Wang and Y.-W. Yang, Superstructure-Induced Hierarchical Assemblies for Nanoconfined Photocatalysis, *Angew. Chem. Int. Ed.*, 2023, **62**, e202313358.

18 T. Zhao, J. Yi, C. Liu, X. Liang, Y. Shen, L. Wei, X. Xie, W. Wu and C. Yang, "First Come, First Served" and Threshold Effects in a Central-to-Planar-to-Helical Hierarchical Chiral Induction, *Angew. Chem. Int. Ed.*, 2023, **62**, e202302232.

19 H. Zheng, L. Fu, R. Wang, J. Jiao, Y. Song, C. Shi, Y. Chen, J. Jiang, C. Lin, J. Ma and L. Wang, Cation controlled rotation in anionic pillar[5]arenes and its application for fluorescence switch, *Nat. Commun.*, 2023, **14**, 590.

20 X. Tian, S. Li, K. Velmurugan, Z. Bai, Q. Liu, K. Wang, M. Zuo and X.-Y. Hu, A novel photoswitchable AIE-active supramolecular photosensitizer with synergistic enhancement of ROS-generation ability constructed by a two-step sequential FRET process, *Mater. Chem. Front.*, 2023, **7**, 2484-2492.

21 L. Gao, F. Zabihi, S. Ehrmann, S. Hedtrich and R. Haag, Supramolecular nanogels fabricated via host–guest molecular recognition as penetration enhancer for dermal drug delivery, *J. Controlled Release*, 2019, **300**, 64-72.

22 H. Ju, X. Zhou, B. Shi, X. Kong, H. Xing and F. Huang, A pillar[5]arene-based hydrogel adsorbent in aqueous environments for organic micropollutants, *Polym. Chem.*, 2019, **10**, 5821-5828.

23 Z.-Q. Wang, X. Wang and Y.-W. Yang, Pillararene-Based Supramolecular Polymers for Adsorption and Separation, *Adv. Mater.*, 2024, **36**, 2301721.

24 X. Xu, F. A. Jerca, K. Van Hecke, V. V. Jerca and R. Hoogenboom, High compression strength single network hydrogels with pillar[5]arene junction points, *Mater. Horiz.*, 2020, **7**, 566-573.

25 N. Prigyai, T. Bunchuay, A. Ruengsuk, N. Yoshinari, J. Manissorn, P. Pumirat, J. Sapudom, P. Kosiyachinda and P. Thongnuek, Photo-Controlled Reversible Uptake and Release of a Modified Sulfamethoxazole Antibiotic Drug from a Pillar[5]arene Cross-Linked Gelatin Hydrogel, *ACS Appl. Mater. Interfaces*, 2024, **16**, 8250-8265.

26 A. Alsbaiee, B. J. Smith, L. Xiao, Y. Ling, D. E. Helbling and W. R. Dichtel, Rapid removal of organic micropollutants from water by a porous β-cyclodextrin polymer, *Nature*, 2016, **529**, 190-194.

27 A. Meng, J. Xing, Z. Li and Q. Li, Cr-Doped ZnO Nanoparticles: Synthesis, Characterization, Adsorption Property, and Recyclability, *Acs Applied Materials & Interfaces*, 2015, **7**, 27449-27457.

28 X. Lv, D. Xia, Y. Cheng, Y. Liu, J. Zhang, X. Wei and P. Wang, Supramolecular hyperbranched polymer gels based on pillar[5]arene and their applications in removal of micropollutants from water, *Inorg. Chem. Front.*, 2022, **9**, 6248-6257.

29 L. Borah, M. Goswami and P. Phukan, Adsorption of methylene blue and eosin yellow using porous carbon prepared from tea waste: Adsorption equilibrium, kinetics and thermodynamics study, *J. Environ. Chem. Eng.*, 2015, **3**, 1018-1028.

30 H. Dai, Y. Huang and H. Huang, Eco-friendly polyvinyl alcohol/carboxymethyl cellulose hydrogels reinforced with graphene oxide and bentonite for enhanced adsorption of methylene blue, *Carbohydr. Polym.*, 2018, **185**, 1-11.

31 Y. Huang, X. Lee, M. Grattieri, M. Yuan, R. Cai, F. C. Macazo and S. D. Minteer, Modified biochar for phosphate adsorption in environmentally relevant conditions, *Chem. Eng. J.*, 2020, **380**, 122375.

32 D. Gokhale, I. Chen and P. S. Doyle, Micelle-Laden Hydrogel Microparticles for the Removal of Hydrophobic Micropollutants from Water, *ACS Appl. Polym. Mater.*, 2022, **4**, 746-754.

33 M. Saood Manzar, T. Ahmad, N. Ullah, P. Velayudhaperumal Chellam, J. John, M. Zubair, R. J. Brandão, L. Meili, O. Alagha and E. Çevik, Comparative adsorption of Eriochrome Black T and Tetracycline by NaOH-modified steel dust: Kinetic and process modeling, *Sep. Purif. Technol.*, 2022, **287**, 120559.

34 J. Wang and X. Guo, Adsorption kinetic models: Physical meanings, applications, and solving methods, *J. Hazard. Mater.*, 2020, **390**, 122156.

35 R. Scaffaro, A. Maio and M. Gammino, Electrospun polymeric nanohybrids with outstanding pollutants adsorption and electroactivity for water treatment and sensing devices, *Adv. Compos. Hybrid Mater.*, 2024, **7**, 13.

36 J. Xia, Y. Gao and G. Yu, Tetracycline removal from aqueous solution using zirconium-based metal-organic frameworks (Zr-MOFs) with different pore size and topology: Adsorption isotherm, kinetic and mechanism studies, *J. Colloid Interface Sci.*, 2021, **590**, 495-505.

37 R. M. Rego, G. Sriram, K. V. Ajeya, H.-Y. Jung, M. D. Kurkuri and M. Kigga, Cerium based UiO-66 MOF as a multipollutant adsorbent for universal water purification, *J. Hazard. Mater.*, 2021, **416**, 125941.

38 M. Li, X. Ren, Y. Gao, M. Mu, S. Zhu, S. Tian and M. Lu, Constructing bifunctional magnetic porous poly(divinylbenzene) polymer for high-efficient removal and sensitive detection 2024, 35, 109699.

39 A. Silva Gomes, M. Vitória Guimarães Leal, G. Roefero Tolosa, F. Camargo Cabrera, G. Dognani and A. Eloízo Job, Cationic dialdehyde cellulose microfibers for efficient removal of eriochrome black T from aqueous solution, *Bioresour. Technol.*, 2023, **380**, 129096.

40 P. Chen, X. Ma, Z. Zhong, F. Zhang, W. Xing and Y. Fan, Performance of ceramic nanofiltration membrane for desalination of dye solutions containing NaCl and Na2SO4, *Desalination*, 2017, **404**, 102-111.

41 B. M. Babić, S. K. Milonjić, M. J. Polovina and B. V. Kaludierović, Point of zero charge and intrinsic equilibrium constants of activated carbon cloth, *Carbon*, 1999, **37**, 477-481.

42 X. Liu, Y. Wang, R. L. Smith, J. Fu and X. Qi, High-capacity structured MgO-Co adsorbent for removal of phosphorus from aqueous solutions, *Chem. Eng. J.*, 2021, **426**, 131381.

43 M. Zubair, H. A. Aziz, I. Ihsanullah, M. A. Ahmad and M. A. Al-Harthi, Enhanced removal of Eriochrome Black T from water using biochar/layered double hydroxide/chitosan hybrid composite: Performance evaluation and optimization using BBD-RSM approach, *Environ. Res.*, 2022, **209**, 112861.

44 Y. Kaur, T. Jasrotia, R. Kumar, G. R. Chaudhary and S. Chaudhary, Adsorptive removal of eriochrome black T (EBT) dye by using surface active low cost zinc oxide nanoparticles: A comparative overview, *Chemosphere*, 2021, **278**, 130366.
45 I. Khurana, A. K. Shaw, Bharti, J. M. Khurana and P. K. Rai, Batch and dynamic adsorption of Eriochrome Black T from water on magnetic graphene oxide: Experimental and theoretical studies, *J. Environ. Chem. Eng.*, 2018, **6**, 468-477.
46 N. I. Blaisi, M. Zubair, Ihsanullah, S. Ali, T. S. Kazeem, M. S. Manzar, W. Al-Kutti and M. A. Al Harthi, Date palm ash-MgAl-layered double hydroxide composite: sustainable adsorbent for effective removal of methyl orange and eriochrome black-T from aqueous phase, *Environ. Sci. Pollut. Res.*, 2018, **25**, 34319-34331.
47 M. H. Karimi, G. R. Mahdavinia, B. Massoumi, A. Baghban and M. Saraei, Ionically crosslinked magnetic chitosan/κ-carrageenan bioadsorbents for removal of anionic eriochrome black-T, *Int. J. Biol. Macromol.*, 2018, **113**, 361-375.
48 A. M. Skwierawska, M. Bliźniewska, K. Muza, A. Nowak, D. Nowacka, S. E. Zehra Syeda, M. S. Khan and B. Łęska, Cellulose and its derivatives, coffee grounds, and cross-linked, β-cyclodextrin in the race for the highest sorption capacity of cationic dyes in accordance with the principles of sustainable development, *J. Hazard. Mater.*, 2022, **439**, 129588.
49 W. Zhao, K. Feng, H. Zhang, L. Han, Q. He, F. Huang, W. Yu, F. Guo and W. Wang, Sustainable green conversion of coal gangue waste into cost-effective porous multimetallic silicate adsorbent enables superefficient removal of Cd(II) and dye, *Chemosphere*, 2023, **324**, 138287.

The data that support the findings of this study have been included as part of the Supplementary Information.